Applied Mathematical Biosystems, Volume 1, Issue 1, (Jul-Dec 2025), 32-37

Applied Mathematical Biosystems

journal homepage: https://ambjournal.com

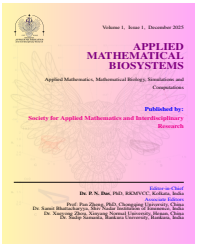

Dynamic Characteristics of Shear-Horizontal Waves in Porous Sandwich Systems

Bikram Dholey[1] **and Abhishek Kanti Biswas**[2]

[1]*Department of Mathematics, Jadavpur University, Kolkata-700032, West Bengal, India*
[2]*Department of Mathematics, Ramakrishna Mission Vivekananda Centenary College, Rahara, Kolkata-700118, West Bengal, India*

Abstract

This paper presents an analytical investigation of shear-horizontal (SH) wave propagation in an inhomogeneous dual-porous layer sandwiched between a viscous sandy medium and a cracked poroelastic half-space. The dual-porous layer is saturated with a heterogeneous fluid and combines both matrix and fracture porosities, enabling a realistic simulation of complicated subsurface formations. The proposed model accounts for material inhomogeneity, solid–fluid interaction, and porous dissipation mechanisms in both the dual-porous layer and the cracked poroelastic medium. Imperfect mechanical interfaces are added at the boundary surfaces to reflect partial bonding conditions, with their consequences defined by nondimensional interfacial stiffness parameters. The influences of interfacial imperfection, fracture volume percentage, porosity, density contrast, and layer thickness ratio on SH-wave dispersion and attenuation are explored in depth. The results demonstrate that both interfacial stiffness and geometrical configuration greatly affect the wave propagation characteristics, revealing the strong sensitivity of SH waves to interfacial circumstances and microstructural features. The established solid–fluid coupled framework gives better physical insight into wave–medium interaction processes and offers a rigorous theoretical basis for nondestructive evaluation, seismic interpretation, and geophysical exploration in layered porous media. features. This solid–fluid coupled theoretical framework provides deeper physical insight into the wave–medium interaction mechanisms and establishes a foundation for nondestructive evaluation, seismic interpretation, and geophysical exploration in layered porous systems.

Keywords: *Shear-horizontal (SH) wave, Dual-porous, Viscous Sandy, Porosity, Classical Spring.*

Corresponding author: Bikram Dholey *E-mail address:* bikram.dholey.563412@gmail.com
Received: October 28, 2025 **Revised:** December 19, 2025 **Accepted:** December 26, 2025 **Published:** December 28, 2025

1. Introduction

In numerous engineering and geophysical applications, such as hydrocarbon extraction, geotechnical analysis, geothermal energy harvesting, and subsurface monitoring, porous geological formations are an essential feature of the Earth's subsurface. In his key articles, Biot [1, 2] laid the theoretical framework for wave propagation in fluid-saturated porous media by carefully analyzing the interaction between an elastic solid frame and a viscous pore fluid. In order to account for the more intricate pore structures and multiscale interactions seen in natural geomaterials, Biot's theory has undergone major extensions and is still a fundamental component of contemporary poromechanics.

A single interconnected pore network is insufficient to fully describe the pore structure in many geological situations. Rather, fractures, joints, vugs, or microcracks are typically overlaid atop a low-permeability matrix that makes up the subsurface. Barenblatt et al. [3] and Warren et al. [4] introduced the double-porosity idea, which treats the matrix and fracture systems as interacting continuum exchanging fluid mass, in order to address the disadvantages of single-porosity models. Later, Berryman and Wang [5, 6] expanded this framework within a rigorous mechanical setting and produced dynamic equations for double-porosity media, allowing for the investigation of transient and wave-induced processes.

Physical properties, including variable fracture density, multiscale permeability, nonlinear fluid–solid coupling, and fracture-dependent anisotropy that are typically encountered in naturally fractured reservoirs, have been integrated in later advances [7–10]. The importance of precisely simulating the interplay between matrix porosity, fracture porosity, and fluid exchange mechanisms under drained and undrained circumstances is also underscored by recent studies [11–16]. These advancements have widened the applicability of porous media theory to modern fields including environmental geophysics, induced seismicity, CO_2 sequestration, and unconventional reservoirs.

In stratified sedimentary basins, where geological compaction and diagenesis typically result in alternating porous, fractured, and low-permeability formations, layered porous and double-porosity structures are especially pertinent. Because of inadequate cementation, thin interfacial fluids, or microcracked transition zones, the interfaces between these layers might not be fully

bonded; instead, they reveal mechanical defects. Partial bonding, interfacial slip, and displacement discontinuities can be successfully modeled using spring-type imperfect interface models, which were first introduced [17] and later used in porous and multilayered media [18]. These models make it possible to systematically measure the impact of interfacial stiffness on wave propagation, which is critical for accurate modeling of geostructural interfaces, designed layered composites, and cracked reservoir systems.

In addition to the classical theories, several recent advances have significantly expanded the modelling capability of porous and double-porosity media, including multiscale formulations done [19–24], wave-induced fluid-flow mechanisms [25–27], and imperfect-interface models for layered or fractured geomaterials [28–39].

Because their motion is only controlled by shear deformations and is particularly sensitive to solid-frame rigidity, fracture density, and interfacial bonding conditions, horizontally polarized shear (SH) waves are especially well-suited to investigating such porous and fractured media. SH-wave analysis in multi-layered porous frameworks has yielded substantial insights into mode conversion, attenuation, and wave dispersion in fluid-saturated formations in recent years [40, 41]. Wave propagation in systems with fracture porosity, matrix porosity, and poor coupling across layers—a configuration typically observed in true subsurface environments—has, however, received very little study.

Inspired by these features, the current study studies SH-wave propagation in a three-layered configuration made up of a higher viscous sandy layer, a finite double-porosity layer, and a bottom fracture half-space. In order to capture genuine interfacial conditions between these distinct porous materials, spring-type imperfect interfaces are created at the layer borders. The generalized double-porosity framework is utilized to develop the governing equations for each layer, and closed-form solutions are discovered to establish the dispersion parameters of guided SH waves. The purpose of this research is to elucidate how porosity, fracture density, solid-fluid coupling, and interfacial stiffness interact to determine how shear waves travel through complicated porous geological media.

2. Formulation of the Model

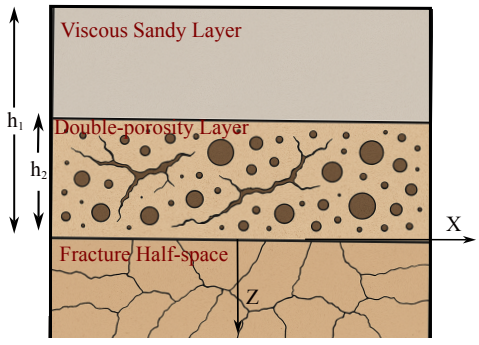

Figure 1. Schematic illustration of the proposed model.

2.1. Dynamics of the Viscous Sandy Layer

For the propagation of shear–horizontal (SH) waves in the viscous sandy layer, the equation of motion can be expressed as [42]

$$\partial_x \tau_{12}^{(s)} + \partial_z \tau_{23}^{(s)} = \rho^{(s)} \partial_{tt} u_2^{(s)}, \tag{1}$$

where the shear stress components are related to the displacement field through [42]

$$\tau_{23}^{(s)} = \mu^{(s)} \partial_z u_2^{(s)}, \qquad \tau_{12}^{(s)} = \eta^{(s)} \mu^{(s)} \partial_x u_2^{(s)}. \tag{2}$$

Here, $\mu^{(s)}$ denotes the rigidity modulus of the sandy layer, $\eta^{(s)}$ is a dimensionless parameter representing shear viscosity, and $\rho^{(s)}$ is the material density.

Assuming harmonic wave motion, we let

$$u_2^{(s)}(x,z,t) = l_1(z)\, e^{ik(x-ct)}, \tag{3}$$

where k is the wave number and c is the common phase velocity of propagation.

To account for the viscous nature of the medium, the effective rigidity modulus $\mu^{(s)}$ is taken as

$$\mu^{(s)} = \mu_0^{(s)} + \mu_1^{(s)} \partial_t, \tag{4}$$

where $\mu_0^{(s)}$ represents the elastic rigidity and $\mu_1^{(s)}$ characterizes the internal frictional resistance of the viscous sandy medium. Substituting Eq. (2) into Eq. (1), the governing equation for SH–wave motion in the viscous sandy layer becomes

$$\mu^{(s)} \left[\eta^{(s)} \partial_{11} u_2^{(s)} + \partial_{33} u_2^{(s)} \right] = \rho^{(s)} \partial_{tt} u_2^{(s)}. \tag{5}$$

Using the harmonic assumption from Eq. (3), Eq. (5) reduces to

$$\frac{d^2 l_1(z)}{dz^2} + k^2 \left[c^2 (\beta^{(s)})^{-2} (1 - i\xi^{(s)})^{-1} - \eta^{(s)} \right] l_1(z) = 0, \tag{6}$$

where the parameters are defined as

$$(\beta^{(s)})^2 = \frac{\mu_0^{(s)}}{\rho^{(s)}}, \qquad \xi^{(s)} = \frac{\mu_1^{(s)}\, k\, c}{\mu_0^{(s)}}. \tag{7}$$

The general solution of Eq. (6) provides the non-vanishing displacement component of the viscous sandy layer as

$$u_2^{(s)}(x,z,t) = \left[A_1 \cos(\Omega^{(s)} z) + A_2 \sin(\Omega^{(s)} z) \right] e^{ik(x-ct)}, \tag{8}$$

where A_1 and A_2 are arbitrary integration constants, and $\Omega^{(s)} = k\sqrt{c^2(\beta^{(s)})^{-2}(1 - i\xi^{(s)})^{-1} - \eta^{(s)}}$.

$$\tau_{23}^{(s)} = \left[-A_1 \Omega^{(s)} \sin(\Omega^{(s)} z) + A_2 \Omega^{(s)} \cos(\Omega^{(s)} z) \right] e^{ik(x-ct)} \tag{9}$$

2.2. Dynamics of the Dual–Porous Layer

Following [6], the equations of motion for a fluid–saturated fractured porous layer are written as [43]

$$\begin{aligned}
&\rho_{11}^{(d)} \ddot{u}_2^{(d)} + \rho_{12}^{(d)} \ddot{u}_m^{(d)} + \rho_{13}^{(d)} \ddot{u}_f^{(d)} + \left(\zeta_{12}^{(d)} + \zeta_{13}^{(d)} \right) \dot{u}_2^{(d)} - \zeta_{12}^{(d)} \dot{u}_m^{(d)} - \zeta_{13}^{(d)} \dot{u}_f^{(d)} \\
&\qquad = \tau_{yj,j}^{(d)}, \\
&\rho_{12}^{(d)} \ddot{u}_2^{(d)} + \rho_{22}^{(d)} \ddot{u}_m^{(d)} + \rho_{23}^{(d)} \ddot{u}_f^{(d)} - \zeta_{12}^{(d)} \dot{u}_2^{(d)} + \left(\zeta_{12}^{(d)} + \zeta_{23}^{(d)} \right) \dot{u}_m^{(d)} - \zeta_{23}^{(d)} \dot{u}_f^{(d)} \\
&\qquad = -M_{p,y}^{(d)}, \\
&\rho_{13}^{(d)} \ddot{u}_2^{(d)} + \rho_{23}^{(d)} \ddot{u}_m^{(d)} + \rho_{33}^{(d)} \ddot{u}_f^{(d)} - \zeta_{13}^{(d)} \dot{u}_2^{(d)} - \zeta_{23}^{(d)} \dot{u}_m^{(d)} + \left(\zeta_{13}^{(d)} + \zeta_{23}^{(d)} \right) \dot{u}_f^{(d)} \\
&\qquad = -F_{p,y}^{(d)}.
\end{aligned} \tag{10}$$

where $u_2^{(d)}, u_m^{(d)}, u_f^{(d)}$ denote the solid displacement, matrix-pore fluid displacement, and fracture–pore fluid displacement, respectively; $\rho_{ij}^{(d)}$ and $\zeta_{ij}^{(d)}$ are the mass coefficients and viscous coupling coefficients.

The macroscopic pressures satisfy

$$M_p^{(d)} = V_m^{(d)}\Phi_m^{(d)} m_p^{(d)}, \qquad F_p^{(d)} = V_f^{(d)}\Phi_p^{(d)} f_p^{(d)}, \tag{11}$$

where $V_m^{(d)} + V_f^{(d)} = 1$, and $\Phi_m^{(d)}$, $\Phi_f^{(d)}$ is the matrix and crack porosity. Tortuosity vectors are denoted by $\tau_t^{(d)}, \tau_m^{(d)}, \tau_f^{(d)}$.

The constitutive relations for the cracked porous medium [6] are expressed as

$$\begin{pmatrix} \tau_{11}^{(d)} \\ \tau_{22}^{(d)} \\ \tau_{33}^{(d)} \\ -m_p^{(d)} \\ -f_p^{(d)} \\ \tau_{23}^{(d)} \\ \tau_{31}^{(d)} \\ \tau_{12}^{(d)} \end{pmatrix} = \begin{bmatrix} \mathbf{N}^{(d)} & \mathbf{0} \\ \mathbf{0} & 2G^{(d)}\mathbf{I} \end{bmatrix} \begin{pmatrix} \nu_{11}^{(d)} \\ \nu_{22}^{(d)} \\ \nu_{33}^{(d)} \\ -m_w^{(d)} \\ -f_w^{(d)} \\ \nu_{23}^{(d)} \\ \nu_{31}^{(d)} \\ \nu_{12}^{(d)} \end{pmatrix}, \tag{12}$$

where $n_{ij}^{(d)}$ are poroelastic coefficients, $G^{(d)}$ is the shear modulus, $\tau_{ij}^{(d)}$ are Stress components and $\nu_{11}^{(d)}$ are strain components and $N_{ij}^{(d)}$ are drained elastic moduli, defined by

$$\mathbf{N}^{(d)} = \begin{pmatrix} N_{11}^{(d)} & N_{12}^{(d)} & N_{13}^{(d)} & n_{14}^{(d)} & n_{15}^{(d)} \\ N_{21}^{(d)} & N_{22}^{(d)} & N_{23}^{(d)} & n_{24}^{(d)} & n_{25}^{(d)} \\ N_{31}^{(d)} & N_{32}^{(d)} & N_{33}^{(d)} & n_{34}^{(d)} & n_{35}^{(d)} \\ n_{41}^{(d)} & n_{42}^{(d)} & n_{43}^{(d)} & n_{44}^{(d)} & n_{45}^{(d)} \\ n_{51}^{(d)} & n_{52}^{(d)} & n_{53}^{(d)} & n_{54}^{(d)} & n_{55}^{(d)} \end{pmatrix}.$$

The fluid contents in matrix pore and fracture pore satisfy [43]

$$m_w^{(d)} = -V_m^{(d)}\Phi_m^{(d)}\nabla\cdot(u_m^{(d)} - u_2^{(d)}), \quad f_w^{(d)} = -V_f^{(d)}\Phi_p^{(d)}\nabla\cdot(u_f^{(d)} - u_2^{(d)}). \tag{13}$$

The displacement components are written as

$$\{u_2^{(d)}, u_m^{(d)}, u_f^{(d)}\} = \{l_2(z),\, l_3(z),\, l_4(z)\}\, e^{i(kx-\omega t)}. \tag{14}$$

By applying exponential variations in $G^{(d)}(z)$, $\rho_{ij}^{(d)}(z)$, and $\zeta_{ij}^{(d)}(z)$, and using Eqs. (10)-(14), the solid displacement is

$$u_2^{(d)} = \left(A_3 e^{\eta_1^{(d)} z} + A_4 e^{\eta_2^{(d)} z}\right) e^{i(kx-\omega t)}, \tag{15}$$

where

$$\eta_1^{(d)} = \frac{-\alpha^{(d)} + i\sqrt{4\gamma^{(d)} - (\alpha^{(d)})^2}}{2}, \qquad \eta_2^{(d)} = \frac{-\alpha^{(d)} - i\sqrt{4\gamma^{(d)} - (\alpha^{(d)})^2}}{2}. \tag{16}$$

$$\gamma^{(d)} = \frac{\bar{\rho}^{(d)}\omega^2}{\bar{G}^{(d)}} - k^2,$$

$$\bar{\rho}^{(d)} = \bar{\rho}_{11}^{(d)} + \frac{i}{\omega}\left(\bar{\zeta}_{12}^{(d)} + \bar{\zeta}_{13}^{(d)}\right) - \frac{\left(\bar{\rho}_{12}^{(d)} - \frac{i}{\omega}\bar{\zeta}_{12}^{(d)}\right)^2}{\bar{\rho}_{22}^{(d)} + \frac{i}{\omega}\bar{\zeta}_{12}^{(d)}} - \frac{\left(\bar{\rho}_{13}^{(d)} - \frac{i}{\omega}\bar{\zeta}_{13}^{(d)}\right)^2}{\bar{\rho}_{33}^{(d)} + \frac{i}{\omega}\bar{\zeta}_{13}^{(d)}}. \tag{17}$$

2.3. Dynamics of the Fracture Half-space

In this section, the porous fracture layer obtained from the double–porosity reduction is treated as an effective single–porosity poroelastic medium containing the solid skeleton displacement $u_2^{(f)}(x,z,t)$ and the fracture–fluid displacement $U_2^{(f)}(x,z,t)$. Following the reduced constitutive structure of the double–porosity model, we introduce the averaged mass coefficients $\rho_{11}^{(f)}$, $\rho_{22}^{(f)}$, $\rho_{12}^{(f)}$, the viscous-drag coefficient $b_{12}^{(f)}$, the effective shear modulus $\bar{G}_f$, and the poroelastic parameters $\bar{K}_u^{(f)}, \bar{K}^{(f)}, \bar{B}^{(f)}$. The increment of fluid content in the fracture pores is denoted by $\bar{\zeta}_f$, and $e^{(f)}$ is the volumetric strain of the fracture skeleton.

The effective stress–strain–pressure relations for the fracture layer read

$$\tau_{ii}^{(f)} = \left(\bar{K}_u^{(f)} - \frac{2}{3}\bar{G}_f\right) e^{(f)} - \bar{K}_u^{(f)}\bar{B}^{(f)}\bar{\zeta}_f + 2\bar{G}_f\bar{e}_{ii}^{(f)}, \tag{18}$$

$$\tau_{ij}^{(f)} = 2\bar{G}_f\,\bar{e}_{ij}^{(f)}, \tag{19}$$

$$-\bar{p}_f = \bar{K}_u^{(f)}\bar{B}^{(f)}e^{(f)} - \frac{\bar{K}_u^{(f)}\bar{B}^{(f)}}{\bar{K}_u^{(f)} - \bar{K}^{(f)}}\,\bar{\zeta}_f. \tag{20}$$

The dynamic balance of linear momentum for the solid and fracture–fluid phases is expressed in matrix form as

$$\begin{pmatrix} \rho_{11}^{(f)} & \rho_{12}^{(f)} \\ \rho_{12}^{(f)} & \rho_{22}^{(f)} \end{pmatrix} \begin{pmatrix} \ddot{u}_2^{(f)} \\ \ddot{U}_2^{(f)} \end{pmatrix} + \begin{pmatrix} b_{12}^{(f)} & -b_{12}^{(f)} \\ -b_{12}^{(f)} & b_{12}^{(f)} \end{pmatrix} \begin{pmatrix} \dot{u}_2^{(f)} \\ \dot{U}_2^{(f)} \end{pmatrix} = \begin{pmatrix} \bar{G}_f\nabla^2 u + \left(\bar{K}_u^{(f)} + \frac{1}{3}\bar{G}_f\right)\nabla e^{(f)} + \bar{B}^{(f)}\bar{K}_u^{(f)}\nabla\bar{\zeta}_f \\ \bar{K}_u^{(f)}\bar{B}^{(f)}\nabla e^{(f)} - \dfrac{\bar{B}^{(f)}\bar{K}_u^{(f)}}{\bar{K}_u^{(f)} - \bar{K}^{(f)}}\nabla\bar{\zeta}_f \end{pmatrix}. \tag{21}$$

The left-hand side includes the solid–fluid inertial coupling and the Darcy-type viscous drag, whereas the right-hand side contains the shear restoring force, volumetric effects, and pore–fluid coupling.

For a horizontally polarized shear (SH) wave propagating along x, the tangential displacements of the solid and fracture fluid are assumed in the time-harmonic form

$$u_2^{(f)}(x,z,t) = l_5(z)\, e^{i(kx-\omega t)}, \qquad U_2^{(f)}(x,z,t) = l_6(z)\, e^{i(kx-\omega t)}. \tag{22}$$

Substituting (22) into the governing system From (21), one can obtain

$$\begin{pmatrix} -\omega^2\rho_{11}^{(f)} - i\omega b_{12}^{(f)} & -\omega^2\rho_{12}^{(f)} + i\omega b_{12}^{(f)} \\ -\omega^2\rho_{12}^{(f)} + i\omega b_{12}^{(f)} & -\omega^2\rho_{22}^{(f)} - i\omega b_{12}^{(f)} \end{pmatrix} \begin{pmatrix} l_5(z) \\ l_6(z) \end{pmatrix} = \begin{pmatrix} \bar{G}_f\dfrac{d^2 l_5(z)}{dz^2} - k^2\bar{G}_f l_5(z) \\ 0 \end{pmatrix}. \tag{23}$$

Equation (23) simplifies to the single second-order ODE

$$\frac{d^2 l_5(z)}{dz^2} + m_1^2\, l_5(z) = 0, \tag{24}$$

where the effective vertical wavenumber m_1 is given by

$$m_1 = \sqrt{-k^2 + \frac{\omega^2\rho_{11}^{(f)} + i\omega b_{12}^{(f)}}{\bar{G}_f} - \frac{(\omega^2\rho_{12}^{(f)} - i\omega b_{12}^{(f)})^2}{\bar{G}_f\,(\omega^2\rho_{22}^{(f)} + i\omega b_{12}^{(f)})}}. \quad (25)$$

The general solution of (24) is

$$l_5(z) = A_5 e^{im_1 z} + A_6 e^{-im_1 z}, \quad (26)$$

and the corresponding fracture–fluid displacement is

$$l_6(z) = \frac{-\omega^2\rho_{12}^{(f)} + i\omega b_{12}^{(f)}}{\omega^2\rho_{22}^{(f)} + i\omega b_{12}^{(f)}}\, l_5(z). \quad (27)$$

Hence, the solid displacement field in the fracture half-space becomes

$$u_2^{(f)}(x,z,t) = A_6 e^{-im_1 z} e^{i(kx-\omega t)}. \quad (28)$$

3. Boundary Conditions

The mechanical boundary conditions applied to the layered medium are specified at the upper free surface $z = -h_1$ and at the interface $z = -h_2$ between the adjoining layers.

At the upper surface $z = -h_1$, the Stress-free condition:

$$\tau_{23}^{(s)} = 0. \quad (29)$$

At the interface $z = -h_2$, continuity conditions due to the presence of a spring type interface becomes:

$$\tau_{23}^{(s)} = \alpha_1\,(u_2^{(s)} - u_2^{(d)}). \quad (30)$$

$$\tau_{23}^{(s)} = \tau_{23}^{(d)}. \quad (31)$$

Again, at the interface $z = 0$, continuity conditions due to the presence of a spring type interface becomes:

$$\tau_{23}^{(d)} = \alpha_2\,(u_2^{(d)} - u_2^{(f)}). \quad (32)$$

$$\tau_{23}^{(d)} = \tau_{23}^{(f)}. \quad (33)$$

To derive the dispersion relation, the displacement and shear stress solutions for each layer are inserted into the relevant boundary and interfacial conditions. The traction-free condition at the upper surface and the spring-type imperfect continuity conditions at the fracture-porous and porous-matrix interfaces create a system of linear algebraic equations in the unknown amplitude constants that is the same throughout. One can write these equations in the compact matrix form as:

$$\mathbf{MA} = \mathbf{0}, \quad (34)$$

where

$$\mathbf{A} = \begin{bmatrix} A_1 & A_2 & A_3 & A_4 & A_6 \end{bmatrix}^T,$$

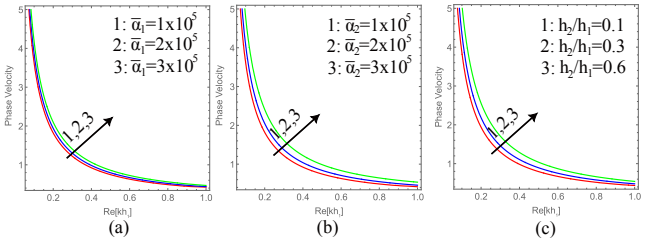

Figure 2. Scaled phase velocity $\frac{c}{\beta^{(s)}}$ versus scaled wave number $\mathrm{Re}(kH)$.

and the non-vanishing components of $\mathbf{M}$ are

$$\begin{aligned}
M_{11} &= \sin(\Omega^{(s)}h_1),\\
M_{12} &= \cos(\Omega^{(s)}h_1),\\
M_{21} &= \Omega^{(s)}\sin(\Omega^{(s)}h_2) - \alpha_1\cos(\Omega^{(s)}h_2),\\
M_{22} &= \Omega^{(s)}\cos(\Omega^{(s)}h_2) + \alpha_1\sin(\Omega^{(s)}h_2),\\
M_{23} &= \alpha_1 e^{-\eta_1^{(d)}h_2},\\
M_{24} &= \alpha_1 e^{-\eta_2^{(d)}h_2},\\
M_{31} &= \Omega^{(s)}\sin(\Omega^{(s)}h_2),\\
M_{32} &= \Omega^{(s)}\cos(\Omega^{(s)}h_2),\\
M_{33} &= -\bar{G}^{(d)}\eta_1^{(d)} e^{-(\alpha^{(d)}+\eta_1^{(d)})h_2},\\
M_{34} &= -\bar{G}^{(d)}\eta_2^{(d)} e^{-(\alpha^{(d)}+\eta_2^{(d)})h_2},\\
M_{43} &= \bar{G}^{(d)}\eta_1^{(d)} - \alpha_2, \qquad M_{44} = \bar{G}^{(d)}\eta_2^{(d)} - \alpha_2, \qquad M_{45} = \alpha_2,\\
M_{53} &= \bar{G}^{(d)}\eta_1^{(d)}, \qquad M_{54} = \bar{G}^{(d)}\eta_2^{(d)}, \qquad M_{55} = im_1\bar{G}_f.
\end{aligned} \quad (35)$$

Now, for non-trivial wave solutions to exist, the determinant of the coefficient matrix $\mathbf{M}$ must equal zero, which represents the necessary dispersion relation that governs shear-horizontal wave propagation in a multilayered double-porosity medium with imperfect interfaces.

4. Numerical analysis

The impact of geometric configuration and interfacial stiffness on SH–wave propagation in the considered multilayered system is shown in Figures 2 and 3. For different values of the non-dimensional spring constants $\bar{\alpha}_1$ and $\bar{\alpha}_2$, which describe the bonding conditions at the upper and lower interfaces, respectively, the scaled phase velocity c/c_1 is plotted against the scaled wavenumber $\mathrm{Re}(kH)$ in Fig. 2. Higher phase velocities result from an increase in either $\bar{\alpha}_1$ or $\bar{\alpha}_2$, suggesting that stiffer interfaces enable more efficient shear-horizontal wave transmission across the layers. The thickness ratio h_2/h_1 has an impact as well. Higher values of h_2/h_1 lead to stronger dispersive behavior and, as a result, lower phase velocities because of increased microstructural interaction within the dual-porous layer. The dispersive nature of SH–waves in fluid-saturated porous composites is supported by the curves' consistent monotonic decay with increasing wavenumber.

The corresponding variation of the attenuation coefficient $\log(\delta)$ with respect to $\mathrm{Re}(kH)$ is shown in Figure 3. As the interfacial stiffness parameters $\bar{\alpha}_1$ and $\bar{\alpha}_2$ increase, the attenuation

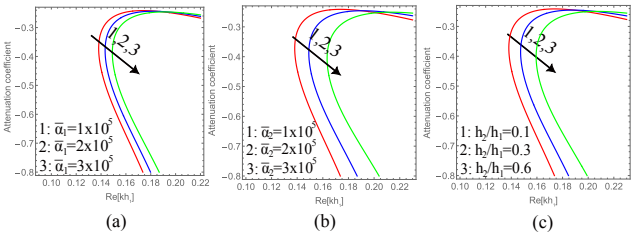

Figure 3. Attenuation coefficient $\log \delta$ versus scaled wave number $\mathrm{Re}(kH)$.

decreases, indicating that better bonding at the interfaces lowers energy dissipation and improves wave penetration across the layered structure. Also, a thicker dual-porous layer results in a higher thickness ratio h_2/h_1, which causes loss in too attenuation. Together, these patterns demonstrate how strongly dispersion and attenuation characteristics depend on interfacial integrity and layer geometry, highlighting the crucial role that boundary and microstructural features play in controlling SH-wave behavior in complex porous media.

5. Conclusion

The study's numerical results unequivocally show that in the suggested multilayered dual-porous system, SH-wave dispersion and attenuation are determined by both geometric configuration and interfacial stiffness. Improved bonding at the interfaces is represented by higher values of the non-dimensional spring constants, which continuously raise phase velocity and decrease attenuation, enabling more effective wave transmission between the layers. On the other hand, because of stronger solid–fluid coupling and viscous interactions within the dual-porous medium, an increase in the thickness ratio amplifies attenuation and intensifies dispersive effects. These results demonstrate how SH-wave propagation is intrinsically sensitive to fluid–solid interactions, interface conditions, and microstructural characteristics.

The proposed model provides a practical framework for geophysical exploration, subsurface characterization, reservoir monitoring, and non-destructive assessment of fluid-saturated layered formations. It takes into account dual-porosity, viscous sandy behavior, and imperfect interfacial bonding. The model offers important insights into wave–medium interactions in heterogeneous geological settings by capturing the intricate interactions between microstructural porosity, fracture interactions, and interface imperfections. Anisotropic material properties, frequency-dependent interfacial behavior, nonlinear fluid–solid coupling, and 3D wave propagation effects could all be added to this framework in future studies. Additionally, the model could be validated using laboratory tests or field-scale seismic observations. These extensions would increase SH-wave analysis's predictive power and expand its use in intricate porous environments.

Acknowledgment

The authors are grateful to their respective institutions for providing excellent facilities to carry out this research work. They also sincerely thank the learned reviewer for their valuable comments and constructive suggestions, which have greatly enriched and improved the quality of this manuscript.

REFERENCES

[1] M. A. Biot. Theory of propagation of elastic waves in a fluid-saturated porous solid. i. low-frequency range. *Journal of the Acoustical Society of America*, 28:168–178, 1956.

[2] M. A. Biot. Theory of propagation of elastic waves in a fluid-saturated porous solid. ii. higher frequency range. *Journal of the Acoustical Society of America*, 28:179–191, 1956.

[3] G. I. Barenblatt, Iu. P. Zheltov, and I. N. Kochina. Basic concepts in the theory of seepage of homogeneous liquids in fissured rocks. *Journal of Applied Mathematics and Mechanics*, 24:1286–1303, 1960.

[4] J. E. Warren and P. J. Root. The behavior of naturally fractured reservoirs. *SPE Journal*, pages 245–255, 1963.

[5] J. G. Berryman and H. F. Wang. The elastic coefficients of double-porosity models for fluid transport in fractured rock. *Journal of Geophysical Research*, 100:24611–24627, 1995.

[6] J. G. Berryman and H. F. Wang. Elastic wave propagation and attenuation in a double-porosity dual-permeability medium. *International Journal of Rock Mechanics and Mining Sciences*, 37:63–78, 2000.

[7] J. M. Carcione. *Wave Fields in Real Media: Wave Propagation in Anisotropic, Anelastic, Porous and Electromagnetic Media*. Elsevier, 2014.

[8] Sharmistha Rakshit, Kshitish Ch Mistri, Amrita Das, and Anirban Lakshman. Mathematical analysis of rayleigh-type wave propagation in a thermo-porous piezoelectric composite structure with interfacial imperfection employing dual-phase-lag model. *Mathematics and Mechanics of Solids*, 0(0):10812865251334809, 2025. . URL https://doi.org/10.1177/10812865251334809.

[9] Amrita Das, Nikhil Chand, and Kshitish Ch. Mistri. Modelling and analysis of love-type wave propagation in ortho-viscoelastic and ortho-piezoelectric media with imperfect spring-double membrane interfaces. *Physica Scripta*, 100(9):095205, 2025. .

[10] Swarnava Kundu, Amrita Das, and Kshitish Ch. Mistri. Sh-waves in a complex fluid composite structure with spring membrane imperfect interfaces. *ZAMM – Journal of Applied Mathematics and Mechanics / Zeitschrift für Angewandte Mathematik und Mechanik*, 2024. .

[11] C. Lyu, J. Luo, and W. Cheng. Wave propagation in double-porosity media revisited. *Geophysical Journal International*, 198:1690–1705, 2014.

[12] Sharmistha Rakshit, Anirban Lakshman, and Kshitish Ch Mistri. Analysis of different wave characteristics in a fiber-reinforced thermo-piezoelectric rotating medium influenced by gravity. *Waves in Random and Complex Media*, 0(0):1–31, 2024. .

[13] Amrita Das, Abhishek Kumar Singh, Prajnya Parimita Patel, Kshitish Ch. Mistri, and Amares Chattopadhyay. Reflection and refraction of plane waves at the loosely bonded common interface of piezoelectric fibre-reinforced and fibre-reinforced composite media. *Ultrasonics*, 94:131–144, 2019. ISSN 0041-624X. . URL https://www.sciencedirect.com/science/article/pii/S0041624X18302671.

[14] Attenuation and dispersion of sh-waves in a loosely bonded sandwiched fluid saturated porous layer. *Soil Dynamics and Earthquake Engineering*, 107:350–362, 2018. ISSN 0267-7261. .

[15] Sharmistha Rakshit, Kshitish Ch. Mistri, Amrita Das, and Anirban Lakshman. Effect of interfacial imperfections on

sh-wave propagation in a porous piezoelectric composite. *Mechanics of Advanced Materials and Structures*, 29(25): 4008–4018, 2022. .

[16] Sharmistha Rakshit, Kshitish Ch Mistri, Amrita Das, and Anirban Lakshman. Stress analysis on the irregular surface of visco-porous piezoelectric half-space subjected to a moving load. *Journal of Intelligent Material Systems and Structures*, 33(10):1244–1270, 2022. .

[17] N. A. Haskell. The dispersion of surface waves on multilayered media. *Bulletin of the Seismological Society of America*, 43:17–34, 1953.

[18] M. Schoenberg. Elastic wave behavior across linear slip interfaces. *Journal of the Acoustical Society of America*, 68: 1516–1521, 1980.

[19] J. Ba, T. C. M. Zhang, J. M. Carcione, and Z. Z. Huang. Biot–rayleigh theory of wave propagation in double-porosity media. *Journal of Geophysical Research: Solid Earth*, 116 (B6):B06202, 2011.

[20] C. Boutin. On models of double porosity poroelastic media. *Geophysical Journal International*, 203(3):1694–1725, 2015.

[21] L. Zhang, Y. Guo, and J. Liu. Wave propagation in infinituple-porosity media. *Journal of Geophysical Research: Solid Earth*, 126(3):e2020JB021266, 2021.

[22] Y. Kang, J. Ba, and J. M. Carcione. A multiscale model for wave propagation in double-porosity media including macro-, meso- and microscopic wave-induced fluid flow. *International Journal of Engineering Science*, 190:104932, 2025.

[23] C. C. Parra, O. Umnova, and E. Gourdon. Acoustic wave propagation in gas-saturated double-porosity permeo-elastic materials with resonant mesopores. *Acta Mechanica Sinica*, 41(x):1–18, 2025.

[24] B. Dholey and K. Mistri. Shear-horizontal wave dynamics in smart fiber composites with layerwise interfacial imperfections. *Boletim da Sociedade Paranaense de Matemática*, 43, 2025. .

[25] M. D. Sharma and R. S. Chattopadhyay. Effect of local fluid flow on the propagation of elastic waves in a double-porosity solid. *Geophysical Journal International*, 200(3):1423–1442, 2015.

[26] N. Li, W. Deng, L.-Y. Fu, J. M. Carcione, and T. Han. Wave propagation in double-porosity thermoelastic media. *Geophysics*, 87(5):T213–T229, 2022.

[27] W. Chen, X. Wang, and Y. Zhang. Modeling seismic wave propagation in partially saturated porous media with multiscale squirt-flow mechanisms. *Frontiers in Earth Science*, 13:1610897, 2025.

[28] B. Dholey, A. Alneamy, K. Mistri, S. Guha, and M. Tharwan. The influence of sh-wave propagation in a tri-layered composite structure with interfacial imperfections. *Journal of Vibration Engineering & Technologies*, 13(2):197, 2025. . URL https://doi.org/10.1007/s42417-025-01776-y.

[29] M. Serpilli, M. I. Borino, and A. Piccolroaz. Interface models in coupled thermoelasticity: spring-layer, coherent and general imperfect interfaces. *Technologies*, 9(1):17, 2021.

[30] X.-Q. Fang, H.-L. Wang, and J. Wu. Dynamic response of a non-circular lined tunnel with viscoelastic imperfect interface in a poroelastic medium. *International Journal of Solids and Structures*, 112:62–77, 2017.

[31] Y. Tan, M. Yang, and X. Li. Dynamic response of a circular lined tunnel with an imperfect interface embedded in an unsaturated poroelastic medium under p wave. *Computers and Geotechnics*, 122:103514, 2020.

[32] K. Liu, H. Wu, and Y. Jiang. Dynamic responses of transversely isotropic and layered elastic media with imperfect interfaces under moving loads. *International Journal of Non-Linear Mechanics*, 156:104432, 2024.

[33] S.-Y. Zhang, Q. Huang, and X. Xu. Evanescent waves in hybrid poroelastic metamaterials with interface effects. *International Journal of Heat and Mass Transfer*, 201:123596, 2023.

[34] S. Kundu and S. K. Tomar. Impacts on the propagation of sh-waves in a heterogeneous viscoelastic layer sandwiched between an anisotropic porous layer and an initially stressed half-space. *Journal of Mechanics*, 33(6):833–849, 2017.

[35] N. Zhang, X. Wang, and P. Wang. Effect of interfacial imperfections on sh-wave propagation in a porous piezoelectric composite. *Journal of Intelligent Material Systems and Structures*, 32(14):1595–1610, 2021.

[36] Y. Liu and R. K. Gupta. Propagation of love-type wave in an imperfectly bonded layered poroelastic structure. *International Journal of Geomechanics*, 22(11):04022287, 2022.

[37] R. Dutta and A. K. Sinha. Comparative analysis of double- and single-porosity effects on sh-wave propagation in elastic layers with void pores. *Soil Dynamics and Earthquake Engineering*, 184:107322, 2024.

[38] P. Venkatesan and Z. Alam. Study of sh-wave regulation through a multilayered model of poroelastic and inhomogeneous media. *Journal of Vibration and Control*, 31 (x):1–22, 2025.

[39] J. Zhao, H. Li, and S. K. Singh. Sh-waves in a complex fluid composite structure with spring-type imperfect interfaces. *Zeitschrift für Angewandte Mathematik und Mechanik*, 104 (10):e202301024, 2024.

[40] A. Kumar and P. K. Sharma. Shear wave propagation in porous multilayered structures. *Soil Dynamics and Earthquake Engineering*, 129:105971, 2020.

[41] R. Sharma and S. K. Tomar. Dispersion of sh waves in porous strata with imperfect interfaces. *Journal of Applied Geophysics*, 191:104369, 2021.

[42] Abhishek Kumar Singh, Kshitish Ch. Mistri, and Amrita Das. Propagation of sh-wave in a corrugated viscous sandy layer sandwiched between two elastic half-spaces. *Waves in Random and Complex Media*, 27(2):213–240, 2017. .

[43] Shishir Gupta, Rachaita Dutta, and Soumik Das. Love-Type wave propagation in an inhomogeneous cracked porous medium loaded by heterogeneous viscous liquid layer. *Journal of Vibration Engineering & Technologies*, 9(3):433–448, April 2021.